Electronic Supplementary Material (ESI) for Dalton Transactions.

Support Information

NiCoP/MXene nanocomposites via electrostatic self-assembly for high-performance supercapacitor electrodes

Shuling Liu*, Ying Li, Wei Zhang, Jie Wang, Wenxuan Xu,Chao Wang

College of Chemistry & Chemical Engineering, Shaanxi Key Laboratory of Chemical Additives for Industry, Shaanxi University of Science & Technology, Xi'an, 710021, PR China

Contents:

1. Electrochemical Measurements
2. Material characterization
3. Supplementary figures S1-S8
4. Supplementary tables S1-S4
5. Supplementary References

1. Electrochemical Measurements

The specific capacity (Cs, C g^{-1}) of the electrode material can be obtained from the galvanostatic charge-discharge curve by the following formula:[1]

$$C_S = \frac{I \times \Delta t}{m} \tag{1}$$

Where *I* is the discharge current (A), Δt is the discharge time (s), and *m* represents the mass of the active material coated on the carbon cloth (g).

Asymmetric supercapacitor (ASC) was assembled using NiCoP/MXene composites and commercial activated carbon (AC) as positive electrode and negative electrode. In order to balance the potential of the two electrodes, the mass ratio of the positive and negative materials must satisfy the following formula:[2]

$$\frac{m_+}{m_-} = \frac{C_- \Delta V_-}{C_+ \Delta V_+} \tag{2}$$

Where m (g) is the mass of the electrode active material, C (C g^{-1}) is the specific capacitance of a single electrode, ΔV is the potential window of the positive electrode and the negative electrode, and the mass ratio of the positive electrode and the negative electrode is calculated to be 1:5.24. The corresponding energy density (E, Wh kg^{-1}) and power density (P, W kg^{-1}) can be obtained by the following two formulas:[3]

$$E = \frac{C \times \Delta V^2}{2 \times 3.6} \tag{3}$$

$$P = \frac{3600 \times E}{\Delta t} \tag{4}$$

2. Material characterization

The phase structure of the NiCoP/MXene composite was characterized by Bruker D8 advanced X-ray powder diffractometer with Cu Ka radiation (λ = 1.5418 Å). The surface morphology and energy spectrum (EDS) of the samples were analyzed by field emission scanning electron microscopy (SEM, FE-SEM, Hitachi S-4800, Japan). The microstructure of the samples was characterized using transmission electron microscopy (TEM, FEI Tecnai G^2F20, USA). The elemental composition and valence states of the samples were analyzed by X-ray photoelectron spectroscopy (XPS, UK AXIS SUPRA (Kratos)).

3. Supplementary figures

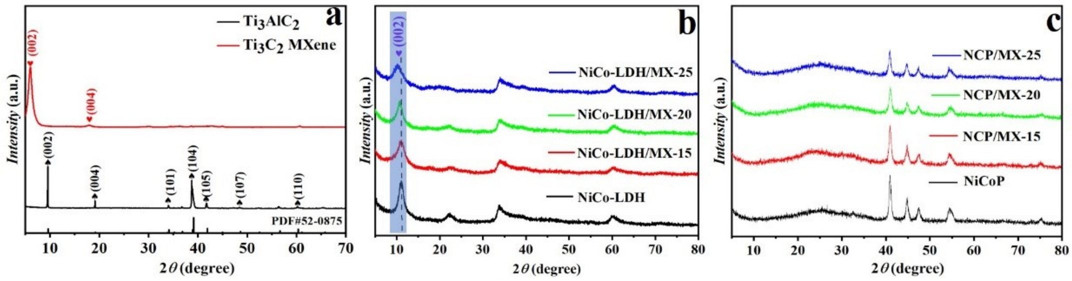

Figure S1. (a) XRD patterns of Ti_3AlC_2 and Ti_3C_2 MXene; (b, c) XRD patterns of NiCo-LDH precursors and NiCoP with different masses of MXene nanosheets added.

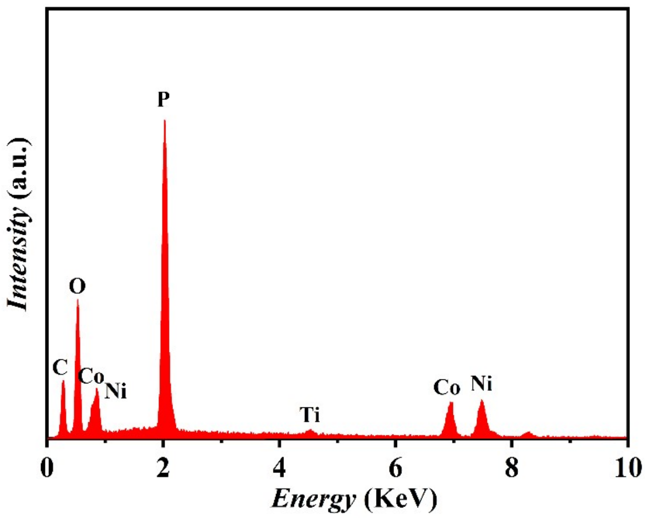

Figure S2. EDS spectrum of NCP/MX-20.

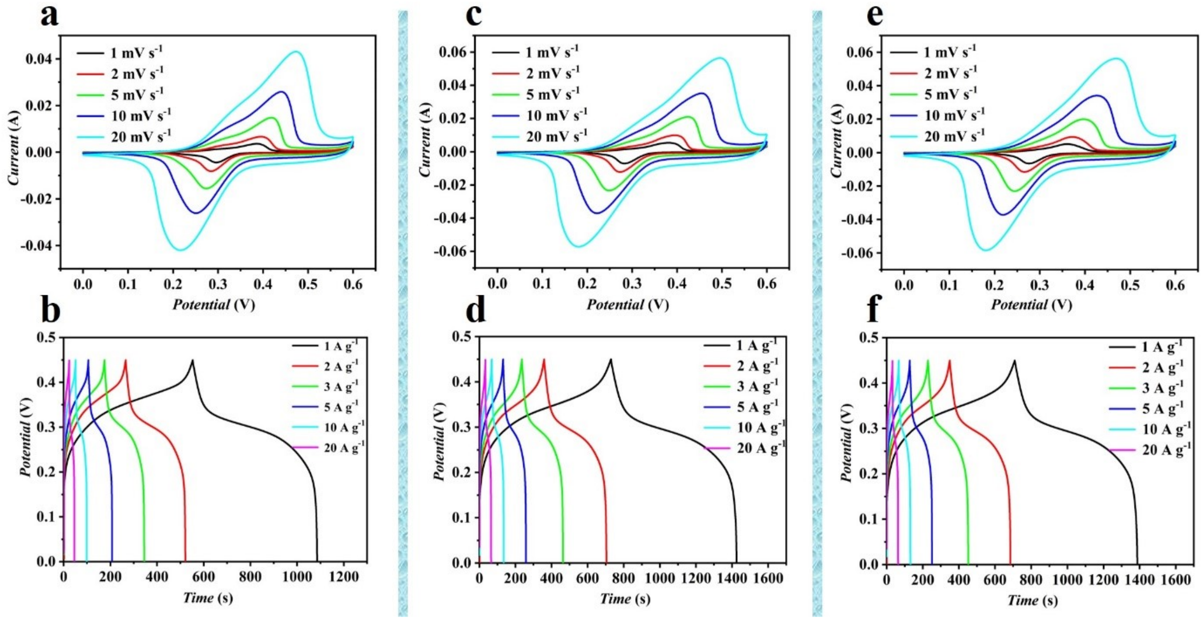

Figure S3. (a, c and e) CV curves of the NiCoP, NCP/MX-15 and NCP/MX-25 at different scan rates; (b, d and f) GCD curves of the NiCoP, NCP/MX-15 and NCP/MX-25 at different current densities.

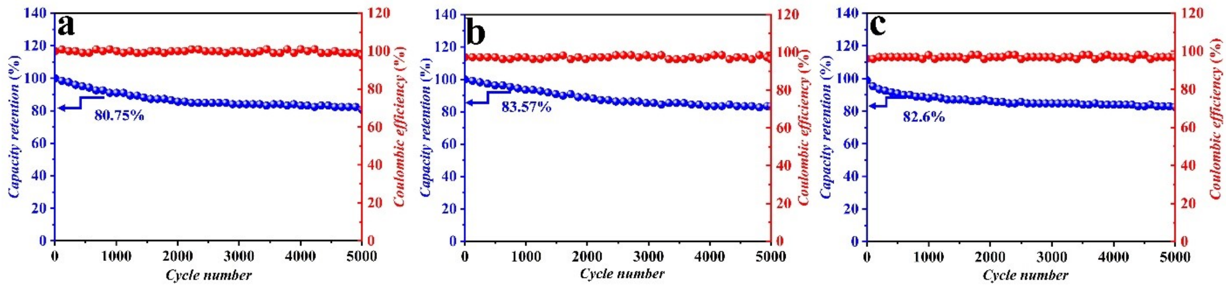

Figure S4. (a, b and c) Cycling performance of the NiCoP, NCP/MX-15 and NCP/MX-25 electrode within 5000 cycles at 10 A g^{-1}.

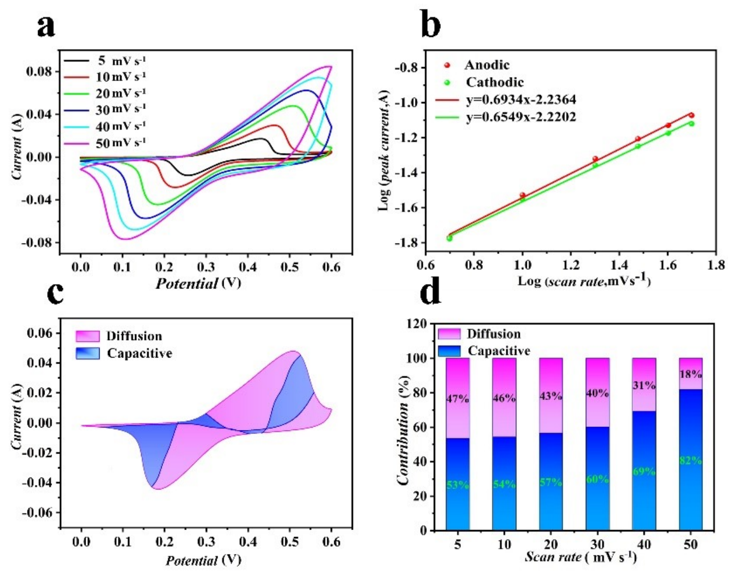

Figure S5. (a) CV curves of NiCoP electrode at different scan rates; (b) the relationship between log(v) and log(i) of NiCoP electrode at different scan rates; (c) distribution of diffusion and capacitive contribution of NiCoP electrode at 20 mV s^{-1} and (d) contribution rate of diffusion and capacitive control behavior of NiCoP electrodes at different scan rates.

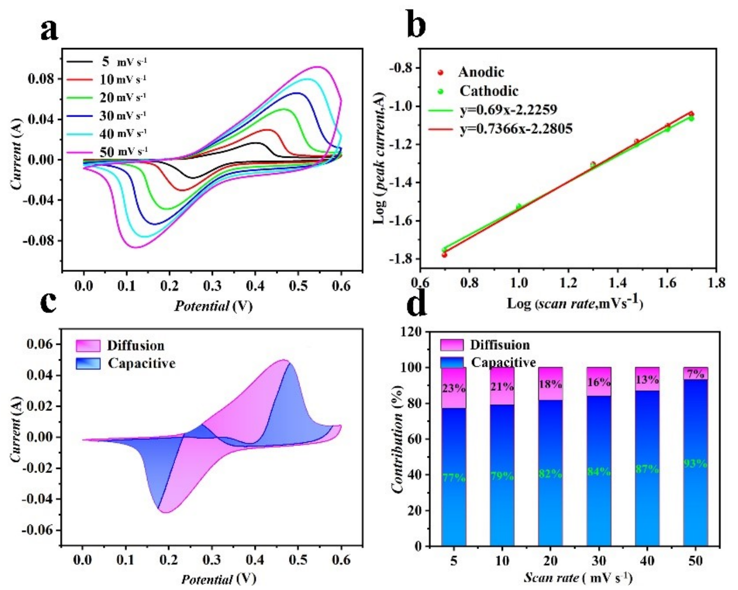

Figure S6. (a) CV curves of NCP/MX-15 electrode at different scan rates; (b) the relationship between log(v) and log(i) of NCP/MX-15 electrode at different scan rates; (c) distribution of diffusion and capacitive contribution of NCP/MX-15 electrode at 20 mV s^{-1} and (d) contribution rate of diffusion and capacitive control behavior of NCP/MX-15 electrodes at different scan rates.

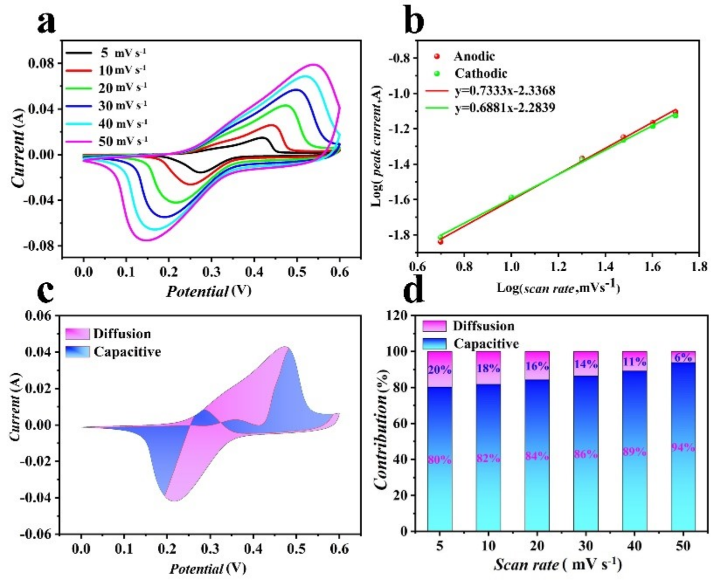

Figure S7. (a) CV curves of NCP/MX-25 electrode at different scan rates; (b) the relationship between log(v) and log(i) of NCP/MX-25 electrode at different scan rates; (c) distribution of diffusion and capacitive contribution of NCP/MX-25 electrode at 20 mV s^{-1} and (d) contribution rate of diffusion and capacitive control behavior of NCP/MX-25 electrodes at different scan rates.

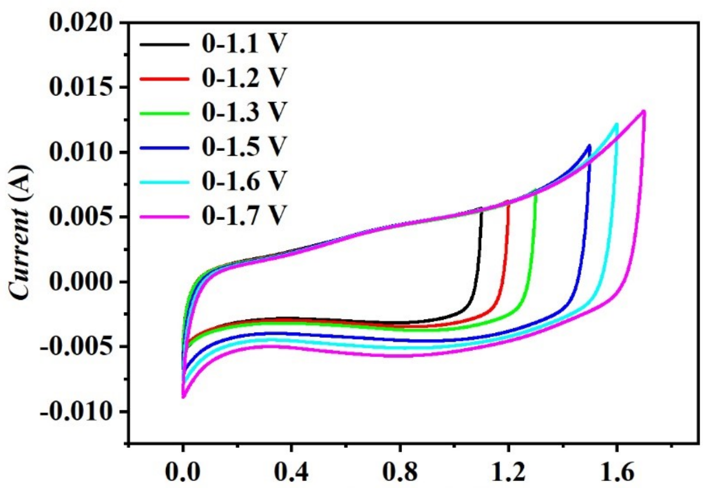

Figure S8. CV curves of the NCP/MX-20//AC ASC at different voltage windows at a scan rate of 20 mV s^{-1}.

4. Supplementary tables S1-S4

Table S1. The NCP/MX-20 of elemental composition of Smart quant results by the EDS.

Element	*Wt%*	*At%*
PK	45.57	61.23
NiK	30.54	21.66
CoK	22.49	15.89
TiK	1.4	1.22

Table S2. The specific capacititance (C g^{-1}) at different current densities in Figure 3e.

	1 A g^{-1}	**2 A g^{-1}**	**3 A g^{-1}**	**5 A g^{-1}**	**10 A g^{-1}**	**20 A g^{-1}**
NiCoP	532.67	510.42	509	508.53	482.99	444
NCP/MX-15	696.83	691.32	683.74	672.55	652	618
NCP/MX-20	848.83	844.69	842.69	830.05	807.02	764
NCP/MX-25	677.93	659.14	656.94	645.54	622.99	582

Table S3. Comparison of the capacity performance of as-prepared NCP/MX-20 and battery-type electrode materials reported previously.

Electrode material	Morphology	Specific capacity	Current density	Ref
NiCoP/C	nanoparticles	775.87 C g^{-1}	1 A g^{-1}	4
NiCoP/NC	hollow nanocages	1127 F g^{-1}	1 A g^{-1}	5
NiCoP@CoS	tree-like core-shell nanoarrays	1796 F g^{-1}	2 A g^{-1}	6
Cu-NiCoP	nanocages	800 C g^{-1}	1 A g^{-1}	7
NiCoP/NiCo-OH	hierarchical cactus-like	1100 F g^{-1}	1 A g^{-1}	8

Ni-Co-P/POx	Sea-urchin-like	647 C g^{-1}	1 A g^{-1}	9
NiCoP/MLG	porous flower-like	1419.6 F g^{-1}	1 A g^{-1}	10
N-CNTs@NiCoP/CoP	Hetero-nanosheets	152 mAh g^{-1} (547.2 C g^{-1})	1 A g^{-1}	11
NiCoP	porous nanosheet	1142.84 F g^{-1}	1 A g^{-1}	12
LDH-MXene	nanosheets	983.6 F g^{-1}	2 A g^{-1}	13
NiCoP	nanoparticles	1456 F g^{-1}	2 A g^{-1}	14
Ni-CoP@C@CNT	nanorods	708.1 F g^{-1}	1 A g^{-1}	15
NiCoP-4-500	hollow nano cubes	1590 F g^{-1}	1 A g^{-1}	16
O-NiCoP	porous nanosheets	1663.2 F g^{-1}	1 A g^{-1}	17
NiCoP-MOF	lamellar brick-stacked	728 C g^{-1}	1 A g^{-1}	18
Ni_2P / NiCoP	nanoparticles	741.3 C g^{-1}	1 A g^{-1}	19
NCP/MX-20	porous flower-like	848.8 C g^{-1} (1886.2 Fg^{-1})	1 A g^{-1}	This work

Table S4. Fitted parameters of the Nyquist plots in Fig. 3f using equivalent circuits.

samples	R_s (Ω)	R_{ct} (Ω)
NiCoP	1.125	0.23
NCP/MX-15	0.664	0.12
NCP/MX-20	0.46	0.13
NCP/MX-25	0.71	0.19

5. Supplementary References

1 S. Hou, X. Xu, M. Wang, Y. Xu, T. Lu, Y. Yao, L. Pan, Carbon-incorporated Janus-type Ni_2P/Ni hollow spheres for high performance hybrid supercapacitors, *J. Mater. Chem. A*, 2017, **5,** 19054-19061.

2 M. Shang, J. Zhang, X. Liu, Y. Liu, S. Guo, S. Yu, S. Filatov, X. Yi, N, S self-doped hollow-sphere porous carbon derived from puffball spores for high performance supercapacitors, *Appl. Surf. Sci.*, 2021, **542,** 148697.
3 T. Dang, G. Zhang, Q. Li, Z. Cao, G. Zhang, H. Duan, Ultrathin hetero-nanosheets assembled hollow Ni-Co-P/C for hybrid supercapacitors with enhanced rate capability and cyclic stability, *J. Colloid Interface Sci.*, 2020, **577,** 368-378.
4 Q. Zhou, Y. Gong, K. Tao, Calcination/phosphorization of dual Ni/Co-MOF into NiCoP/C nanohybrid with enhanced electrochemical property for high energy density asymmetric supercapacitor, *Electrochim Acta*, 2019, **320,** 134582.
5 T. Zhao, C. Liu, F. Yi, X. Liu, A. Gao, D. Shu, J. Ling, Promoting high-energy supercapacitor performance over NiCoP/N-doped carbon hybrid hollow nanocages via rational architectural and electronic modulation, *Appl. Surf. Sci.*, 2021, **569,** 151098.
6 Z. Xu, C. Du, H. Yang, J. Huang, X. Zhang, J. Chen, NiCoP@CoS tree-like core-shell nanoarrays on nickel foam as battery-type electrodes for supercapacitors, *Chem. Eng. J.* 421, 2021, **421,** 127871.
7 L. Lyu, W. Hooch Antink, B.-H. Lee, C.W. Kim, E. Jung, K.-d. Seong, T. Hyeon, Y. Piao, Zeolitic Imidazole Framework Sacrificial Template-Assisted Synthesis of NiCoP Nanocages Doped with Multiple Metals for High-Performance Hybrid Supercapacitors, *ACS Appl. Energy Mater.*, 2021, **4,** 10553-10564.
8 X. Li, H. Wu, A.M. Elshahawy, L. Wang, S.J. Pennycook, C. Guan, J. Wang, Cactus-like NiCoP/NiCo-OH 3D architecture with tunable composition for high-performance electrochemical capacitors, *Adv. Funct. Mater.*, 2018, **28,** 1800036.
9 H.C. Chen, S. Jiang, B. Xu, C. Huang, Y. Hu, Y. Qin, M. He, H. Cao, Sea-urchin-like nickel–cobalt phosphide/phosphate composites as advanced battery materials for hybrid supercapacitors, *J. Mater. Chem. A*, 2019, **7,** 6241-6249.
10 M. Shuai, J. Lin, W. Wu, H. Kuang, W. Zhang, Q. Ling, H. Chen, S. Komarneni, Metallic nickel–cobalt phosphide/multilayer graphene composite for high-performance supercapacitors, *New J. Chem.*, 2020, **44,** 8796-8804.
11 T. Dang, D. Wei, G. Zhang, L. Wang, Q. Li, H. Liu, Z. Cao, G. Zhang, H. Duan, Homologous NiCoP/CoP hetero-nanosheets supported on N-doped carbon nanotubes for high-rate hybrid supercapacitors, *Electrochim Acta*, 2020, **341,** 135988.
12 Q. Liu, R. Hu, J. Qi, Y. Sui, Y. He, Q. Meng, F. Wei, Y. Ren, Facile synthesis of NiCoP nanosheets on carbon cloth and their application as positive electrode material in asymmetric supercapacitor, *Ionics*, 2020, **26,** 355-366.

13 H. Li, F. Musharavati, E. Zalenezhad, X. Chen, K. Hui, K. Hui, Electrodeposited NiCo layered double hydroxides on titanium carbide as a binder-free electrode for supercapacitors, *Electrochim Acta*, 2018, **261,** 178-187.
14 S. Kavian, S. Hajati, M. Moradi, High-rate supercapacitor based on NiCo-MOF-derived porous NiCoP for efficient energy storage, *J. Mater. Sci.: Mater. Electron.*, 2021, **32,** 13117-13128.
15 J. Gu, L. Sun, Y. Zhang, Q. Zhang, X. Li, H. Si, Y. Shi, C. Sun, Y. Gong, Y. Zhang, MOF-derived Ni-doped CoP@C grown on CNTs for high-performance supercapacitors, *Chem. Eng. J.*, 2020, **385,** 123454.
16 M. Wang, J. Zhong, Z. Zhu, A. Gao, F. Yi, J. Ling, J. Hao, D. Shu, Hollow NiCoP nanocubes derived from a Prussian blue analogue self-template for high-performance supercapacitors, *J. Alloys Compd.*, 2022, **893,** 162344.
17 Y. Zhang, L. Sun, L. Zhang, X. Li, J. Gu, H. Si, L. Wu, Y. Shi, C. Sun, Y. Zhang, Highly porous oxygen-doped NiCoP immobilized in reduced graphene oxide for supercapacitive energy storage, *Composites, Part B*, 2020, **182,** 107611.
18 S. He, F. Guo, Q. Yang, H. Mi, J. Li, N. Yang, J. Qiu, Design and fabrication of hierarchical NiCoP–MOF heterostructure with enhanced pseudocapacitive properties, *Small*, 2021, **17,** 2100353.
19 Z. Li, K. Ma, F. Guo, C. Ji, H. Mi, P. Qiu, H. Pang, Construction of homologous Ni_2P/NiCoP heterostructure for enhanced pseudocapacitive properties, *Mater. Lett.*, 2021, **288,** 129319.